Check for updates

Electrospun ZIF-67/PVDF composite membranes for efficient ciprofloxacin removal from wastewater†

Ping Li,‡[a] Xiaolin Yue,‡[a] Anhong Li,[b] Can Cui,[a] Lan Wang[a] and Wenyuan Tan ⓘ *[a]

Cobalt 2-methylimidazole (ZIF-67) has been broadly explored for its applications in the treatment of antibiotics in wastewater. However, ZIF-67 in powder form is difficult to recover. In the study, ZIF-67 and Polyvinylidene Fluoride (PVDF) were blended *via* electrospinning to prepare ZIF-67/PVDF membrane for adsorption of ciprofloxacin (CIP). The ZIF-67/PVDF membrane demonstrated outstanding adsorption efficiency for CIP, with a maximum adsorption capability of 4087.5 μg cm^{-2}. The adsorption performance of ZIF-67/PVDF remains stable across a wide pH range and is unaffected by ionic interference. The ZIF-67/PVDF adsorbent follows pseudo-second-order kinetics and the Langmuir model. Furthermore, thermodynamic research indicates the adsorption of CIP is a spontaneous and exothermic process. It is proposed that the adsorption mechanism of CIP onto ZIF-67/PVDF involves electrostatic interactions, hydrogen bonding, $\pi-\pi$ interactions, coordination bonding, and hydrophobic interactions.

1. Introduction

Ciprofloxacin (CIP), a fluoroquinolone antibiotic, is widely used in the prevention and treatment of bacterial infections as well as in animal husbandry, owing to its broad-spectrum antibacterial activity and low toxicity.[1] However, CIP has a low absorption rate in organisms, with 70–90% remaining unabsorbed and subsequently entering the aquatic environment in the form of the parent drug and metabolites.[2] Studies have shown that CIP is chemically stable and tends to accumulate in water bodies, posing a significant threat to ecosystems. Therefore, the effective removal of CIP from wastewater is of critical importance.

Currently, various materials and methods have been developed for CIP removal from wastewater, including biodegradation,[3–6] advanced oxidation processes,[7–9] and adsorption.[10–14] Among these, adsorption has become a widely adopted method due to its simplicity, cost-effectiveness, and high efficiency. A range of adsorbent materials, such as carbon,[15–17] clay,[18] and Metal–Organic Frameworks (MOFs),[19–23] have been utilized for CIP removal. MOFs, in particular, have gained attention because of their high surface area, tunable pore size, and excellent thermal and chemical stability.[24] Cobalt 2-methylimidazole (ZIF-67), a subclass of MOFs, stands out for its simple synthesis, structural stability, and catalytic activity, making it applicable in various fields. However, ZIF-67 in its powdered form consists of nano-sized particles, which are challenging to recover during water purification processes.[25] In contrast, Polyvinylidene Fluoride (PVDF) membrane is more suitable as an adsorbent because of its membrane structure, which is easy to be recovered by fishing. Nonetheless, PVDF membranes have limited adsorption efficiency due to their lack of active functional groups, which restricts their application in wastewater treatment. To overcome these limitations, MOF materials can be integrated with PVDF membranes to develop composite materials that combine high adsorption efficiency with ease of recovery. For example, Ying Liu and co-workers prepared ZIF-67/PVDF hybrid membranes *via* mechanical blending and the lyotropic phase transition process, demonstrating their potential as effective adsorption materials for wastewater.[26] It has been reported that PVDF and MOF were blended by electrospinning technology.[27]

Therefore, this paper employs electrospinning technology to prepare a ZIF-67/PVDF nanofiber adsorption membrane by blending the MOF material with a PVDF membrane to remove ciprofloxacin from water. The adsorption conditions, including ZIF-67 content and pH, were optimized, and the adsorption thermodynamics, kinetics, and mechanisms were discussed. Additionally, the effect of inorganic salt ions in water on the performance of the adsorption membrane was investigated. The ZIF-67/PVDF nanofiber adsorption membrane was characterized using SEM, XRD, FT-IR, XPS, and WCA.

[a]College of Chemical Engineering, Sichuan University of Science and Engneering, Zigong, Sichuan, 643000, China. E-mail: twyhyx@126.com

[b]College of Chemical and Environmental Engineering, Sichuan University of Science and Engineering, Zigong, Sichuan, 643000, China

‡ Ping Li and Xiaolin Yue contributed to the work equally and should be regarded as co-first authors.

The results show that ZIF-67/PVDF nanofiber has excellent adsorption performance, which is stable in a wide pH range and is not affected by ion interference. The ZIF-67/PVDF nanofiber followed pseudo-second-order kinetics and Langmuir model. The adsorption process of CIP is spontaneous and exothermic. According to the research, the adsorption of CIP on the ZIF-67/PVDF membrane is controlled by a combination of dominant interactions that vary depending on the pH of the solution. When pH < 5.8, there is electrostatic attraction between the negatively charged membrane surface and the positively charged CIP$^+$ molecule. In the medium pH range (5.8–8.2), the hydrophobic interactions[28] and π–π interactions[29,30] between the aromatic rings of ZIF-67 and CIP are the main driving forces for adsorption. When the pH > 8.2, the coordination bonding between the open metal centers of ZIF-67 and the COO$^-$ group of CIP$^-$ is the dominant mechanism.[29] In addition, the hydrogen bonding between ZIF-67 and the -NH group of the neutral CIP molecules are secondary factor.

2. Experimental

2.1 Chemicals and reagents

Polyvinylidene fluoride (PVDF, Sinopharm, 400 000) particles, hexahydrate cobalt nitrate (Co(NO$_3$)$_2$·6H$_2$O, Aladdin, 99.9%), methanol (Macklin, 99.5%), 2-methyl imidazole (Aladdin, 99%), polyvinyl pyrrolidone (Aladdin, K30), N, N-dimethylformamide (DMF, Aladdin, 99.5%), ciprofloxacin (Aladdin, 98%) were of analytical grade and used without further purification.

2.2 Synthesis of the ZIF-67/PVDF composite nanofiber membrane

The entire synthesis process for the membranes is shown in Fig. 1. As reported in the literature,[26] Co(NO$_3$)$_2$·6H$_2$O (0.87 g) and 2-methylimidazole (1.97 g) were each dissolved in methanol, with volumes of 30 mL and 20 mL, respectively. The mixtures were then blended, stirred for 30 minutes, and allowed to stand for 24 hours. The resulting purple powder was collected, washed three times with methanol, and dried at 60 °C for 10 h. Subsequently, ZIF-67 (0.36 g), PVDF (1.8 g), and PVP (90 mg) were dispersed in 20 mL of DMF and stirred for 8 hours. Electrospinning was carried out at an injection speed of 0.6 mL h^{-1} and a voltage of 18 kV. Finally, ZIF-67/PVDF membrane was soaked in methanol for 30 min (ZIF-67/PVDF needs to be activated by the step of soaking methanol before use, while achieving the purpose of removing residual DMF and PVP), and then dried at 60 °C for 2 h.

2.3 Characterization

The morphology of the samples was characterized using a field emission scanning electron microscope (SEM, Hitachi SU-8010, Japan). The phase composition was analyzed by X-ray diffraction (XRD, PANalytical Empyrean, Netherlands). The characteristic functional groups were identified using Fourier transform infrared spectroscopy (FT-IR, Bruker, Germany). The chemical states on the sample surface were examined *via* X-ray photoelectron spectroscopy (XPS, Thermo Scientific K-Alpha, USA). The water contact angle (WCA) was measured using a contact angle measurement device (Biolin Scientific, Sweden).

2.4 Adsorption experiments

Adsorption experiments were conducted at 298.15 K to evaluate adsorption performance of ZIF-67/PVDF membranes. The ciprofloxacin (CIP) concentration after adsorption equilibrium was determined at a wavelength of 277 nm using an ultraviolet-visible spectrophotometer. The effects of inorganic ions and pH on CIP adsorption by ZIF-67/PVDF membranes were also investigated. Detailed procedures for adsorption isotherm, thermodynamic, and kinetic studies are provided in the ESI.† The adsorption capacity was calculated using.[26]

$$Q_e = \frac{(C_0 - C_e)V}{S} \tag{1}$$

where C_0 (mg L^{-1}) is the initial concentration of ciprofloxacin, C_e (mg L^{-1}) is the equilibrium concentration, V (L) is the solution volume, and S (cm^2) is the membrane area.

3. Results and discussion

3.1 Characterizations of ZIF-67/PVDF

The typical morphologies of ZIF-67, PVP/PVDF, ZIF-67/PVDF, and ZIF-67/PVDF-CIP were studied by SEM (Fig. 2). The SEM images reveal ZIF-67 exhibits well-defined rhombohedral
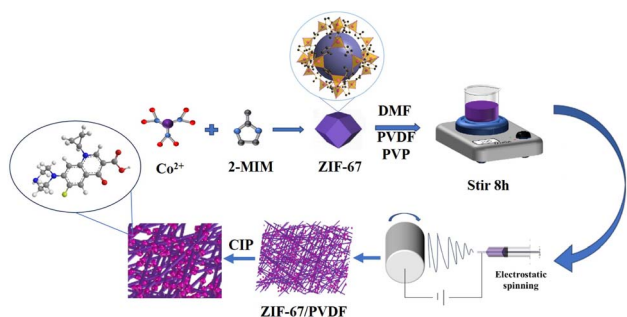

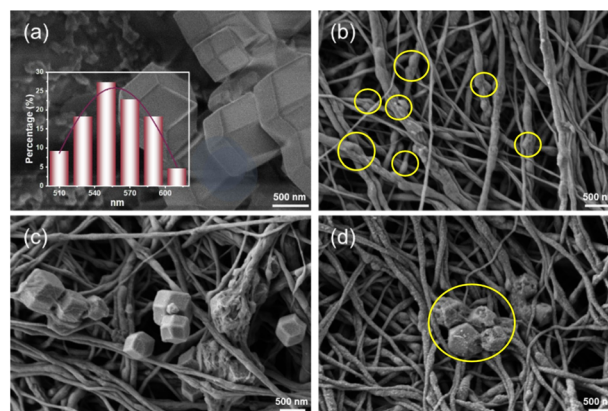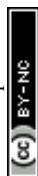**Fig. 1** Preparation of ZIF-67/PVDF membrane and adsorption of CIP.

Fig. 2 SEM of ZIF-67 (a), PVP/PVDF (b), ZIF-67/PVDF (c) and ZIF-67/PVDF–CIP (d).

dodecahedron shape with an average particle size of approximately 554 nm (Fig. 2a), consistent with its characteristic crystalline morphology. On the contrary, the surface of PVP/PVDF nanofibers is non-uniform and contains noticeable bulges, which are likely a result of uneven jetting during the electrospinning process. These imperfections may impact the overall uniformity and mechanical properties of the nanofiber membrane.

The ZIF-67/PVDF membranes demonstrates a combination of structural features from ZIF-67 and PVP/PVDF (Fig. 2c). Specifically, it retains the rhombic dodecahedron structure of ZIF-67 while incorporating the nanofiber matrix of PVP/PVDF. This finding demonstrates that ZIF-67 has been effectively integrated into PVP/PVDF fibers, which facilitates the formation of a composite nanofiber membrane with greater structural complexity. Such hybrid structures are expected to synergistically combine the advantages of ZIF-67's adsorption capacity and the flexibility and stability of the PVP/PVDF matrix.

After the adsorption of ciprofloxacin, significant morphological changes are observed. The rhombic dodecahedron structure of ZIF-67 has changed, likely due to interactions with the adsorbed ciprofloxacin molecules. Furthermore, the previously smooth surface of the ZIF-67/PVDF composite membrane becomes noticeably rougher (Fig. 2d). These particles are attributed to the ciprofloxacin adsorbed onto the membrane surface, indicating successful binding of the target molecule. The observed changes in surface morphology further validate the effective adsorption capability of ZIF-67/PVDF, highlighting its potential for practical applications in pollutant removal.

The characteristic functional groups of ZIF-67/PVDF, PVP/PVDF, and ZIF-67 were studied by FT-IR, as shown in Fig. 3a. In the FT-IR spectrum of ZIF-67, several distinct characteristic peaks were observed: the Co–N bond at 425 cm^{-1},[31–34] C–O stretching vibrations at 992 and 1140 cm^{-1}, N–H bending vibrations at 691 and 753 cm^{-1}, the C–N bond at 1303 cm^{-1}, and the C=C bond at 1422 and 1577 cm^{-1}.[35] These peaks are consistent with the structural features of ZIF-67 and confirm its successful synthesis. For the PVP/PVDF membrane, characteristic peaks corresponding to C–F and C–C bond stretching vibrations in PVDF were observed at 1165 and 1070 cm^{-1}, respectively. In the FT-IR spectrum of ZIF-67/PVDF membrane, the presence of all typical peaks for PVP/PVDF and ZIF-67 membrane indicated that two components had been effectively combined. The presence of these peaks indicates that interaction between PVP/PVDF and ZIF-67 is primarily physical
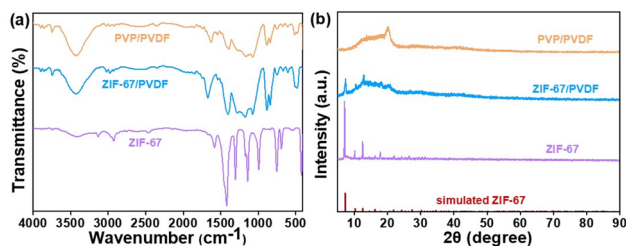
rather than chemical, as no new functional group peaks were detected.

As depicted in Fig. 3b, XRD was utilized to analyze the crystalline structures of ZIF-67/PVDF, PVP/PVDF, and ZIF-67. The diffraction pattern of ZIF-67 exhibited characteristic peaks at 2θ values of 7.10° (001), 10.15° (002), 12.51° (112), 14.49° (022), 16.25° (013), 17.84° (222), 21.98° (114), and 24.34° (233),[26] corresponding to its highly crystalline rhombic dodecahedron structure. In the ZIF-67/PVDF membrane, diffraction peaks corresponding to PVP/PVDF and ZIF-67 the membrane were observed, confirming the coexistence of these two phases within the composite. This result further demonstrates that ZIF-67 has been effectively integrated into PVP/PVDF medium while preserving its crystal structure. The retention of these characteristic peaks suggests that the ZIF-67 crystalline structure remains intact after integration, ensuring that its adsorption properties are preserved in the composite membrane.

The hydrophilicity of the ZIF-67/PVDF, PVP/PVDF, and PVDF membrane was assessed through contact angle measurements, as shown in Fig. 4. PVDF nanofibre membrane is a hydrophobic material (Fig. 4b). For the PVP/PVDF membrane, water droplets penetrated the surface relatively quickly, indicating its inherent hydrophilicity due to the presence of PVP (Fig. 4c). The polar functional groups in PVP facilitate strong interactions with water molecules, promoting rapid wetting. In contrast, the ZIF-67/PVDF composite membrane exhibited a slightly slower wetting process, requiring approximately 35 seconds to achieve complete wetting and zero contact angle (Fig. 4d). This delay can be attributed to the fact that the presence of ZIF-67 reduces the effective pore size of the PVP/PVDF membrane, thereby reducing water permeability. Therefore, a given volume of water needs more time to pass through. Despite this, ZIF-67/PVDF membranes retained outstanding hydrophilicity, suggesting that incorporation of ZIF-67 did not compromise the overall wettability of the composite structure.

The elemental compositions and chemical states of the ZIF-67/PVDF and ZIF-67/PVDF-CIP membranes were analyzed using
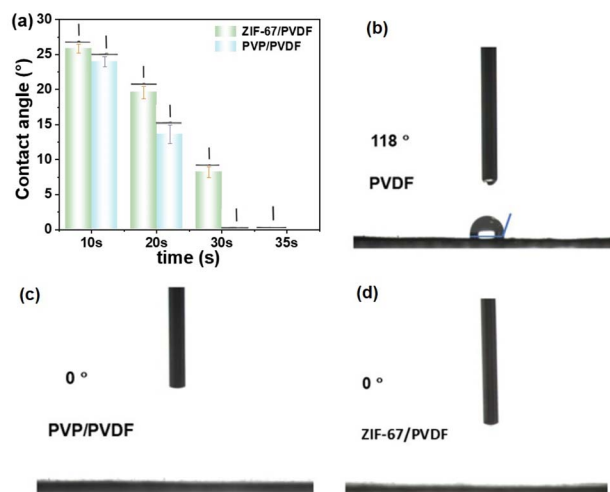
Fig. 3 (a) FT-IR spectra, (b) XRD spectra of ZIF-67, PVDF and ZIF-67/PVDF.

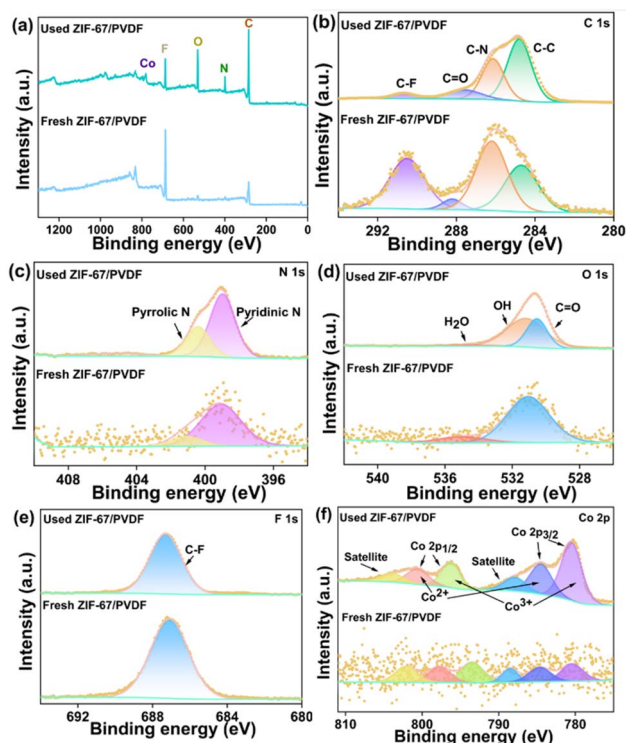Fig. 4 Contact angles of PVDF, PVP/PVDF and ZIF-67/PVDF (a–d).

Fig. 5 XPS spectra of survey (a), C 1s (b), N 1s (c), O 1s (d), F 1s (e) and Co 2p (f) for fresh and used ZIF-67/PVDF.

X-ray photoelectron spectroscopy (XPS). The XPS survey spectra of the two membranes confirm the presence of C, N, O, F, and Co elements (Fig. 5a). As shown in Fig. 5b, the high-resolution C 1s spectrum reveals four distinct peaks located at 284.8, 286.1, 287.6, and 290.7 eV, corresponding to C–C, C–N, C=O, and C–F bonds, respectively. In the N 1s spectrum (Fig. 5c), two peaks are observed at 399.1 and 401.1 eV, which are assigned to pyridinic nitrogen and pyrrolic nitrogen, respectively.[36] The high-resolution O 1s spectrum is presented in Fig. 5d, with two peaks at 531.1 and 535.0 eV, attributed to the C=O group and O–H bonds from water molecules.[29] Notably, after adsorption, a new peak at 531.2 eV appears, which corresponds to the O–H group of ciprofloxacin, confirming its successful adsorption onto the membrane. The F 1s spectrum (Fig. 5e) exhibits a peak at 687.1 eV, attributed to the C–F bond, which originates from the PVDF component. The Co 2p spectrum (Fig. 5f) displays four primary peaks at 780.5, 784.5, 796.3, and 800.6 eV, corresponding to Co $2p_{3/2}$ and Co $2p_{1/2}$ states.[37] Furthermore, weaker satellite peaks are observed at 787.9 and 803.9 eV, further confirming the characteristic electronic structure of cobalt in ZIF-67.

3.2 Adsorption of CIP

The effect of ZIF-67 content in the ZIF-67/PVDF composite membrane on the adsorption of ciprofloxacin (CIP) was evaluated, and the results are presented in Fig. 6. The concentration of adsorption sites within the membrane increases with the ZIF-67 content. The difference in adsorption capacity between 20%
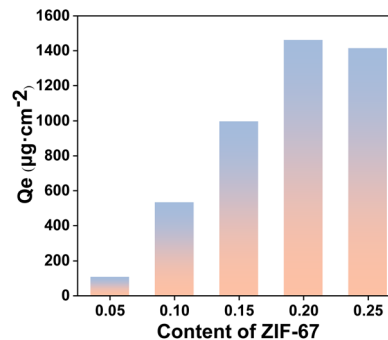

Fig. 6 The addition of ZIF-67 in ZIF-67/PVDF ($T = 298.15$ K, pH = 6–8, C_0 (CIP) = 400 mg L^{-1}, the area of the membrane = 4 cm^2, $t = 15$ h).

and 25% ZIF-67 content is negligible. Therefore, 20% ZIF-67 was chosen as the optimal addition ratio for subsequent experiments to balance performance and material usage.

3.3 Adsorption of kinetic study

The kinetic process of CIP adsorption on the ZIF-67/PVDF membrane was systematically investigated, as depicted in Fig. 7. During the adsorption process, CIP molecules migrated from the solution to the surface of the ZIF-67/PVDF membrane and then diffused into the pore structure of the membrane. The results show that the adsorption equilibrium time and adsorption rate of CIP remained relatively stable across different initial concentrations of ciprofloxacin. This indicates that the adsorption performance of the membrane is not significantly influenced by variations in the initial solute concentration within the tested range, suggesting a robust and efficient adsorption mechanism. To further elucidate the adsorption behavior, pseudo-first-order and pseudo-second-order kinetic models were employed to analyze the adsorption kinetics. The pseudo-first-order and pseudo-second-order kinetic models are shown by eqn (S6) and (S7).† The fitting parameters for both models are summarized in Table 1. The pseudo-second-order kinetic model demonstrated superior fitting performance, with correlation coefficients R^2 ranging from 0.871 to 0.921, which were significantly higher than those of the pseudo-first-order model. In addition, the adsorption capacities calculated by the pseudo-second-order kinetic model (Q_e, cal.) are very similar to the experimental values (Q_e).[38] This
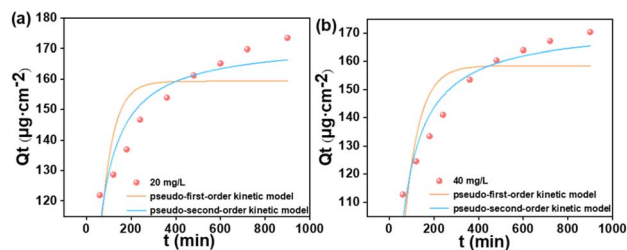

Fig. 7 Pseudo-first-order kinetic model and pseudo-second-order kinetic model of 20 mg L^{-1} (a) and 40 mg L^{-1} (b) of CIP. ($T = 298.15$ K, pH = 6–8, the area of the membrane = 2.25 cm^2, $t = 15$ h).

Table 1 Kinetic fitting parameters

		Pseudo-first-order			Pseudo-second-order		
C_0 mg L^{-1}	Q_e µg cm^{-2}	k_1 (min^{-1})	$Q_{e,cal}$	R^2	k_2 (cm^2 µg^{-1} min^{-1})	$Q_{e,cal}$	R^2
20	173.46	0.018	159.28	0.570	0.00017	172.46	0.871
40	170.36	0.015	158.50	0.685	0.00014	172.95	0.921

result suggests that the pseudo-second-order model more precisely characterizes the adsorption of ciprofloxacin onto the membrane, implying that rate-limiting step is primarily governed by chemical interactions between ZIF-67/PVDF membranes and CIP.[39]

3.4 Adsorption of thermodynamics and isotherm study

The isothermal adsorption curves of ZIF-67/PVDF membranes at 298.15 K, 308.15 K, and 318.15 K are illustrated in Fig. 8. As observed, the equilibrium adsorption capacity of the membranes decreases with increasing temperature, indicating that the adsorption of ciprofloxacin (CIP) on the ZIF-67/PVDF membrane is an exothermic process. To analyze the adsorption mechanism, the experimental data were fitted using the Langmuir and Freundlich models. The Langmuir and Freundlich models are given by eqn (S1)–(S3),† respectively. The fitting parameters for these models are summarized in Table 2. The results reveal that the Langmuir model provides the best fit, with correlation coefficients R^2 ranging from 0.8509 to 0.9086, which are higher than those of the Freundlich model ($R^2 =$ 0.6964–0.7453).

These findings indicate that CIP adsorption on ZIF-67/PVDF membranes are better represented by the Langmuir model, pointing to monolayer adsorption on a consistent surface. Additionally, the favorability of adsorption was evaluated using the separation factor (R_L), where $R_L < 1$ under all three

temperature conditions confirms that the adsorption process is favorable. These findings provide valuable insights into the thermodynamic and kinetic behavior of CIP adsorption on ZIF-67/PVDF membranes, demonstrating their potential for practical applications in water purification under varying thermal conditions.

The adsorption thermodynamic parameters at three different temperatures were calculated by eqn (S4) and (S5),† summarized in Table 3 and illustrated in Fig. 9. The negative value of ΔG^0 ($\Delta G^0 < 0$) indicates that the adsorption of ciprofloxacin (CIP) on the ZIF-67/PVDF membrane is a spontaneous process. The negative value of ΔS^0 ($\Delta S^0 < 0$) suggests that the adsorption process involves a decrease in entropy, likely due to the orderly arrangement of CIP molecules on the membrane surface. Additionally, the negative value of ΔH^0 ($\Delta H^0 < 0$) confirms that the adsorption is exothermic, which is consistent

Table 2 Fitting parameters of isothermal adsorption model

	Langmuir model			Freundlich model		
T (K)	Q_0	R_L	R^2	b	$1/n$	R^2
298.15	4204.3	0.004145	0.9086	1075.9	0.243	0.7453
308.15	3927.1	0.004954	0.8810	917.9	0.251	0.7379
318.15	3937.9	0.01754	0.8509	592.8	0.306	0.6964

Table 3 Adsorption thermodynamic parameter

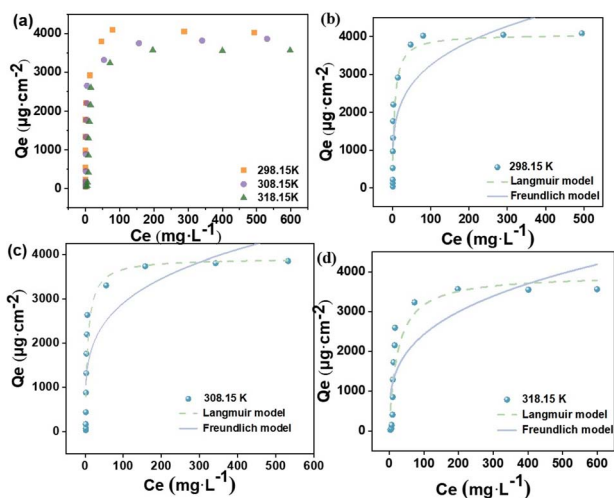| T	$\ln K$	ΔG^0 (kJ mol^{-1})	ΔH^0 (kJ mol^{-1})	ΔS^0 (kJ mol^{-1} K^{-1})
298.15	3.46843	−8.597	−84.525	−0.255
308.15	2.02707	−5.193		
318.15	1.33216	−3.524		

Fig. 8 Effect of temperature on adsorption (a), 298.15 K adsorption isothermal adsorption model (b), 308.15 K adsorption isothermal adsorption model (c), 318.15 K adsorption isothermal adsorption model (d). (pH = 6−8, the area of the membrane = 2.25 cm^2, t = 15 h).
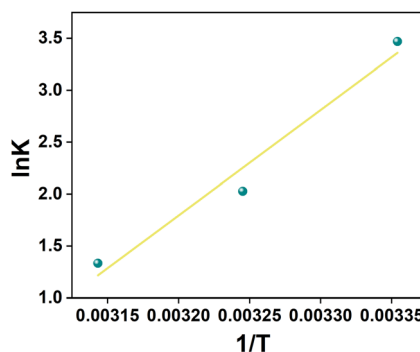

Fig. 9 The relationship between $1/T$ and $\ln K$.

with the experimental observations. The Gibbs free energy change (ΔG^0) values, falling between -20 and 0 kJ mol^{-1}, further confirm that physical adsorption is the dominant mechanism in CIP adsorption on the membrane.

3.5 Effect of pH and inorganic salt ions

The CIP adsorption capacity of ZIF-67/PVDF membranes at different pH levels is presented in Fig. 10a. The adsorption capacity remains relatively stable within the pH range of 4.0–8.0 but decreases sharply as the pH increases from 9.0 to 10.0. These results indicated that the alkaline environment significantly inhibited the adsorption of CIP. This phenomenon may be attributed to the deprotonation reaction of the carboxyl functional group (–COOH) in the CIP molecule, resulting in the presence of CIP in the form of negative ions (CIP$^-$), thereby increasing the electrostatic repulsion with the membrane, especially at higher pH conditions.

In natural water systems, various inorganic salt ions are commonly present, which may influence or interfere with the adsorption process. To evaluate this, the effects of coexisting ions (0.1 mol L^{-1} Na$^+$, K$^+$, Ca^{2+}, SO$_4^{2-}$, and NO$_3^-$) on CIP adsorption capability of ZIF-67/PVDF membrane was analyzed, as depicted in Fig. 10b. Since the anion must be accompanied by equivalent moles of cations, the inorganic salts used in the study of the influence of cations are NaCl, KCl, CaCl$_2$, and the control anion variable is Cl$^-$. When studying the influence of anions, the inorganic salts used are NaNO$_3$ and Na$_2$SO$_4$, and the control cation variable is Na$^+$. The results reveal that cations (Na$^+$, K$^+$, and Ca^{2+}) have minimal impact on adsorption capability, whereas anions SO$_4^{2-}$, and NO$_3^-$ reduce the adsorption capacity. This reduction is likely due to competitive adsorption between these anions and CIP molecules on the membrane surface.

Overall, the influence of inorganic ions on adsorption of CIP is relatively small, suggesting that ZIF-67/PVDF membranes demonstrates excellent stability and selectivity in the presence of coexisting ions. These properties make the membrane a promising candidate for practical water treatment applications, where diverse ions coexist in complex environments.

3.6 Possible adsorption mechanism

The adsorption of CIP onto the ZIF-67/PVDF membrane is governed by a combination of dominant interactions (as
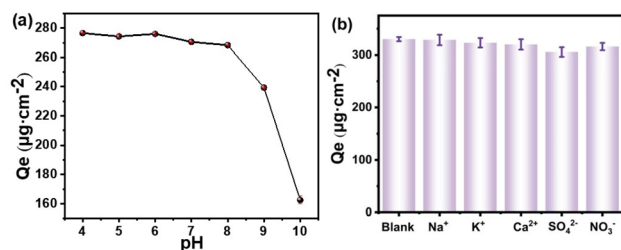

Fig. 10 Effect of pH on adsorption of CIP (a) ($T = 298.15$ K, C_0 (CIP) = 30 mg L^{-1}, the area of the membrane = 2.25 cm^2, $t = 15$ h). Effect of inorganic salt ions on adsorption of CIP (b) ($T = 298.15$ K, pH = 6–8, C_0 (CIP) = 75 mg L^{-1}, the area of the membrane = 2.25 cm^2, $t = 15$ h).
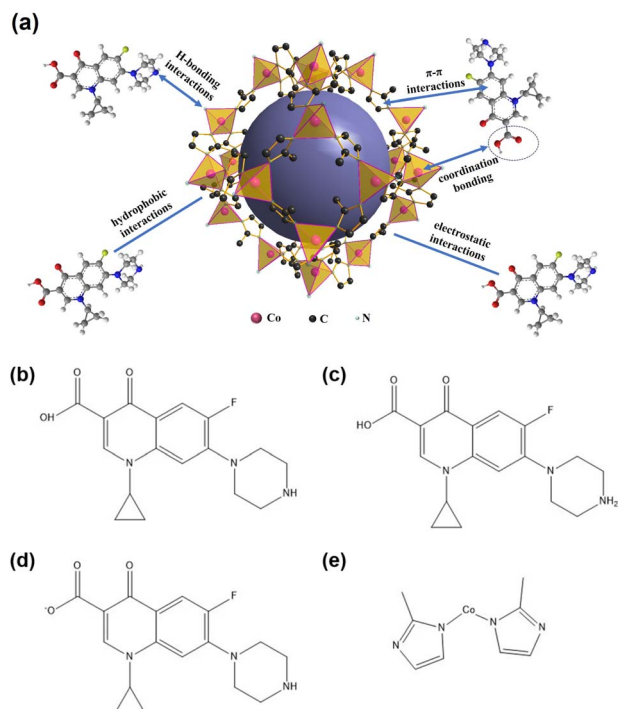

Fig. 11 The possible mechanisms of the adsorption of CIP on the ZIF-67/PVDF (a), structures of CIP$^\pm$ (b), CIP$^+$ (c), CIP$^-$ (d) and ZIF-67 (e).

illustrated in Fig. 11a), which vary depending on the solution pH. Ciprofloxacin exists in different ionic forms depending on the pH of the solution due to its two pK_a values (5.8 and 8.2).[40–42] Fig. S3† shows the CIP status. Simultaneously, the ZIF-67/PVDF membrane surface is negatively charged across the pH range of 4–10.[43] When the pH < 10.6, the surface of ZIF-67 is positively charged.[44] When the pH is lower than 5.8, CIP predominantly exists as a cation (CIP$^+$), and there is electrostatic attraction between the negatively charged membrane surface and the positively charged CIP$^+$ molecule. This is supported by the high adsorption capacity observed under acidic conditions.

When the pH is higher than 8.2, CIP primarily exists as an anion (CIP$^-$), and electrostatic repulsion between the negatively charged membrane and CIP$^-$ reduces adsorption efficiency. However, coordination bonding between the open metal centers of ZIF-67 and the COO$^-$ group of CIP$^-$ becomes the dominant mechanism, as evidenced by XPS analysis, which confirms the formation of metal–oxygen bonds.

In the intermediate pH range (5.8–8.2), where CIP exists in its zwitterionic form (CIP$^\pm$), hydrophobic interactions[28] and π–π interactions[29,30] between the aromatic rings of ZIF-67 and CIP are the main driving forces for adsorption. These interactions are further supported by the pseudo-second-order kinetic model, which indicates that chemical interactions (e.g., complexation) play a significant role.

Additional mechanisms, such as hydrogen bonding between ZIF-67 and the –NH group of neutral CIP molecules, contribute to adsorption but are secondary to the dominant interactions described above. ZIF-67/PVDF membrane exhibit stable adsorption across a range of initial CIP concentrations,

emphasizing their potential for practical utility in water treatment applications.

4. Conclusions

In summary, ZIF-67/PVDF membrane were successfully fabricated by electrospinning. These membranes integrate the easy recovery features of PVDF with the high surface area and abundant active sites of ZIF-67. As a result, the ZIF-67/PVDF membrane demonstrate excellent adsorption capacity for ciprofloxacin, along with convenient separation. The adsorption behavior is consistent with the pseudo-second-order kinetic model and the Langmuir model, demonstrating spontaneity and exothermic characteristics. The mechanism involves monolayer chemisorption, driven primarily by hydrogen bonding, hydrophobic interactions, π–π interactions, electrostatic interactions and coordination bonding. However, the main interaction of adsorption is still unclear. It is suggested that microscopic studies, such as molecular dynamics simulation, could be useful for studying the adsorption mechanism.

Thus, ZIF-67/PVDF membranes shows great potential as an ideal adsorbent for adsorption and removal of CIP from wastewater.

Data availability

All data obtained in this study are presented in the manuscript and ESI.†

Conflicts of interest

There are no conflicts to declare.

Acknowledgements

Notes and references

1 G. F. Zhang, X. Liu, S. Zhang, B. Pan and M. L. Liu, *Eur. J. Med. Chem.*, 2018, **146**, 599–612.
2 Q. Zhou, X. Li, S. Wu, Y. Zhong and C. Yang, *Trends Biotechnol.*, 2021, **39**, 8–11.
3 Z. Li, S. Li, T. Li, X. Gao and L. Zhu, *iScience*, 2022, **25**, 104638.
4 S. Zhou, Y. Jia, H. Fang, C. Jin, Y. Mo, Z. Xiao, N. Zhang, L. Sun and H. Lu, *Water Res.*, 2024, **252**, 121226.
5 N. Kamal, A. K. Saha, E. Singh, A. Pandey and P. C. Bhargava, *J. Hazard. Mater.*, 2024, **470**, 134076.
6 L. J. Pan, J. Li, C. X. Li, X. D. Tang, G. W. Yu and Y. Wang, *J. Hazard. Mater.*, 2018, **343**, 59–67.
7 S. B. Verinda, M. Muniroh, E. Yulianto, N. Maharani, G. Gunawan, N. F. Amalia, J. Hobley, A. Usman and M. Nur, *Heliyon*, 2022, **8**, e10137.
8 T. An, H. Yang, G. Li, W. Song, W. J. Cooper and X. Nie, *Appl. Catal., B*, 2010, **94**, 288–294.
9 S. K. Mondal, A. K. Saha and A. Sinha, *J. Cleaner Prod.*, 2018, **171**, 1203–1214.
10 D. Zheng, M. Wu, E. Zheng, Y. Wang, C. Feng, J. Zou, M. Juan, X. Bai, T. Wang and Y. Shi, *J. Colloid Interface Sci.*, 2022, **625**, 596–605.
11 A. Raheem, N. Rahman and S. Khan, *Langmuir*, 2024, **40**, 12939–12953.
12 W. R. D. N. Sousa, A. R. Oliveira, J. F. Cruz Filho, T. C. M. Dantas, A. G. D. Santos, V. P. S. Caldeira and G. E. Luz, *Water, Air, Soil Pollut.*, 2018, **229**, 125.
13 A. Avcı, İ. İnci and N. Baylan, *Water, Air, Soil Pollut.*, 2019, **230**, 250.
14 H. Mao, S. Wang, J. Y. Lin, Z. Wang and J. Ren, *Chin. J. Environ. Sci. (Beijing)*, 2016, **49**, 179–188.
15 A. Avcı, İ. İnci and N. Baylan, *J. Mol. Struct.*, 2020, **1206**, 127711.
16 X. Zheng, X. He, H. Peng, J. Wen and S. Lv, *Bioresour. Technol.*, 2021, **334**, 125238.
17 J. G. Shang, X. R. Kong, L. L. He, W. H. Li and Q. J. H. Liao, *Int. J. Environ. Sci. Technol.*, 2016, **13**, 2449–2458.
18 N. L. Jorge, M. V. Garrafa, J. M. Romero, M. J. Jorge, L. C. Jorge, M. R. Delfino, Y. V. Meruvia-Rojas, A. Hernandez-Laguna and C. I. Sainz-Diaz, *Molecules*, 2024, **29**, 1760.
19 F. Wei, K. Wang, W. Li, Q. Ren, L. Qin, M. Yu, Z. Liang, M. Nie and S. Wang, *Molecules*, 2023, **28**, 4411.
20 S. Bathula, S. Thottathil and Y. M. Puttaiahgowda, *Macromol. Mater. Eng.*, 2024, **310**, 2400238.
21 Q. Luo, P. Liu, L. Bi, L. Shi, J. Zhou, F. Fang, Q. Lv, H. Fu, X. Li and J. Li, *Sep. Purif. Technol.*, 2024, **332**, 125832.
22 J. Li, G. Li, Y. Wang, C. Wang, L. Zhang and N. Liang, *J. Environ. Chem. Eng.*, 2024, **12**, 113508.
23 M. D. Olawale, A. C. Tella, J. A. Obaleye and J. S. Olatunji, *New J. Chem.*, 2020, **44**, 3961–3969.
24 Y. Guo, L. Zhao, J. Fang, X. Liu, J. Qi and H. Li, *J. Environ. Chem. Eng.*, 2024, **12**, 111901.
25 Y. A. Y. A. Mohammed, A. M. Abdel-Mohsen, Q.-J. Zhang, M. Younas, L.-B. Zhong, J.-C. E. Yang and Y.-M. Zheng, *Chem. Eng. J.*, 2023, **461**, 141972.
26 Y. Liu, N. Wang, Z. Sun, Y. Han, J. Xu, Y. Xu, J. Wu, H. Meng and X. Zhang, *Dalton Trans.*, 2021, **50**, 8927–8937.
27 S. Saghir, S. Zhang, Y. Wang, E. Fu, Z. Xiao, A. H. Zahid and C. Pu, *J. Environ. Chem. Eng.*, 2024, **12**, 113166.
28 S. E. Moradi, A. M. Haji Shabani, S. Dadfarnia and S. Emami, *J. Iran. Chem. Soc.*, 2016, **13**, 1617–1627.
29 M. Lin, J. Wu and Z. Chen, *Appl. Surf. Sci.*, 2024, **652**, 159350.
30 G. Wu, J. Ma, S. Li, J. Guan, B. Jiang, L. Wang, J. Li, X. Wang and L. Chen, *J. Colloid Interface Sci.*, 2018, **528**, 360–371.
31 L. Xu, Y. Xiong, B. Dang, Z. Ye, C. Jin, Q. Sun and X. Yu, *Mater. Des.*, 2019, **182**, 108006.
32 Y. Xue, P. Xiang, H. Wang, Y. Jiang, Y. Long, H. Lian and W. Shi, *J. Mol. Liq.*, 2019, **296**, 111990.

33 S. He, Y. Huang, G. Chen, M. Feng, H. Dai, B. Yuan and X. Chen, *J. Hazard. Mater.*, 2019, **362**, 294–302.

34 J. Wang, C. Ma, X. Mu, X. Zhou, L. He, Y. Xiao, L. Song and Y. Hu, *Chem. Eng. J.*, 2020, **402**, 126221.

35 L. Nie, Y. Yang, S. Xin, C. Fang, H. Chen and N. Kang, *Sep. Purif. Technol.*, 2024, **338**, 126429.

36 N. Lu, H. Lin, G. Li, J. Wang, Q. Han and F. Liu, *J. Membr. Sci.*, 2021, **639**, 119782.

37 C. Liang, X. Zhang, P. Feng, H. Chai and Y. Huang, *Chem. Eng. J.*, 2018, **344**, 95–104.

38 Y. Kong, Y. Zhuang, K. Han and B. Shi, *Colloids Surf., A*, 2020, **588**, 124360.

39 N. Kim, B. Cha, Y. Yea, L. K. Njaramba, S. Vigneshwaran, S. S. Elanchezhiyan and C. M. Park, *Chem. Eng. J.*, 2022, **450**, 138068.

40 L. Meng, C. Zhao, T. Wang, H. Chu and C.-C. Wang, *Sep. Purif. Technol.*, 2023, **313**, 123511.

41 T.-B. Nguyen, V.-A. Thai, C.-W. Chen, C. P. Huang, R.-a. Doong, L. Chen and C.-D. Dong, *Sep. Purif. Technol.*, 2022, **288**, 120719.

42 C. R. Gadipelly, K. V. Marathe and V. K. Rathod, *Sep. Sci. Technol.*, 2018, **53**, 2826–2832.

43 U. Sharma, R. Pandey, S. Basu and P. Saravanan, *Chemosphere*, 2023, **320**, 138075.

44 K. Li, M. Chen, L. Chen, S. Zhao, W. Pan and P. Li, *Heliyon*, 2024, **10**, e36848.